

Highway Traffic State Estimation Using Physics Regularized Gaussian Process: Discretized Formulation

Yun Yuan^a, Zhao Zhang^a, Xianfeng Terry Yang^{*a}

^aDepartment of Civil & Environmental Engineering, University of Utah, Salt Lake City, UT 84112, USA

Abstract

Despite the success of classical traffic flow (e.g., second-order macroscopic) models and data-driven (e.g., Machine Learning - ML) approaches in traffic state estimation, those approaches either require great efforts for parameter calibrations or lack theoretical interpretation. To fill this research gap, this study presents a new modeling framework, named physics regularized Gaussian process (PRGP). This novel approach can encode physics models, i.e., classical traffic flow models, into the Gaussian process architecture and so as to regularize the ML training process. Particularly, this study aims to discuss how to develop a PRGP model when the original physics model is with discrete formulations. Then based on the posterior regularization inference framework, an efficient stochastic optimization algorithm is developed to maximize the evidence lowerbound of the system likelihood. To prove the effectiveness of the proposed model, this paper conducts empirical studies on a real-world dataset which is collected from a stretch of I-15 freeway, Utah. Results show the new PRGP model can outperform the previous compatible methods, such as calibrated physics models and pure machine learning methods, in estimation precision and input robustness.

Keywords: Second-order traffic flow model; traffic state estimation; physics regularized machine learning; multivariate Gaussian process

1. Introduction

In view of the steady increase of the number of vehicles and the occurrence of traffic congestion, traffic management represents an important alternative to improve the performance of traffic systems with limited efforts (Fountoulakis et al., 2017). As a precursive step of traffic management strategies, the full traffic state (i.e. flow, density, and speed) on highways should be estimated from the observed data (i.e. traffic counts, vehicle trajectories, etc.). However, in most cases, traffic state estimation (TSE) models can only utilize limited information from traffic detectors as inputs (Bekiaris-Liberis et al., 2016). Fig. 1 show the real world data from a freeway segment of I-15, Utah, where the TSE should be based on the sparse inputs Fig. 1a-1b to yield the dense outputs Fig. 1c-1d. The data are collected from stationary traffic detectors and are only available in limited locations. In the literature, TSE methods are designed to model traffic dynamics, capture data noise, and predict unobserved spatiotemporal traffic states. For example, macroscopic traffic flow models were proposed based on continuum fluid approximation to describe the aggregated behavior of traffic. Those models can generally be classified into three basic categories: (a) the first-order Lighthill-Whitham-Richards (LWR) model (Lighthill and Whitham, 1955; Richards, 1956), (b) the second-order Payne-Whitham (PW) model (Payne, 1971; Whitham, 1975), and (c) the second-order

Email address: x.yang@utah.edu (Xianfeng Terry Yang*)

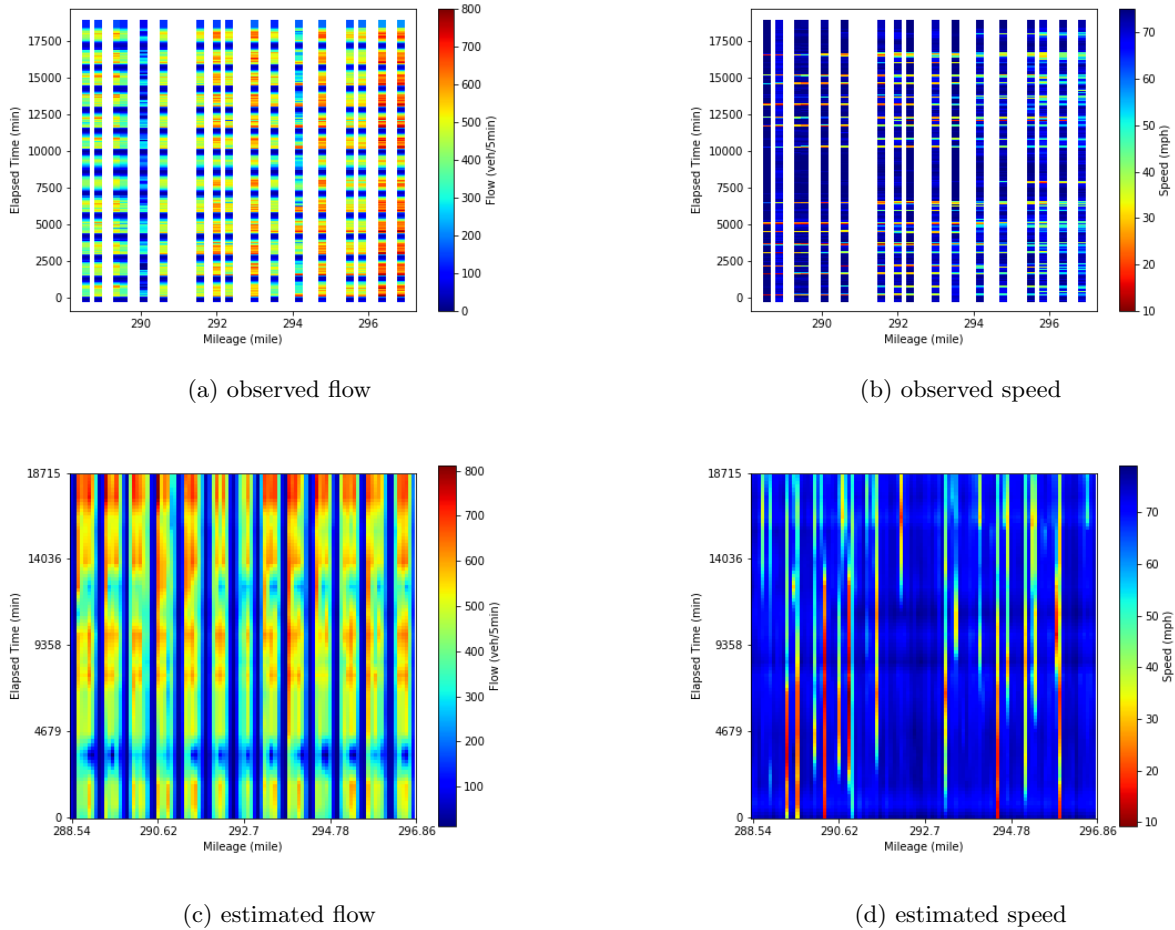


Figure 1: The input and output of traffic state estimation problem

Aw-Rasclé-Zhang (ARZ) model (Aw and Rasclé, 2000; Zhang, 2002). The LWR model succeeds in describing simple behaviors, such as traffic jam and shockwave, however, has limitations in reproducibility of more complex phenomena. Thus, the second-order models, PW and ARZ models, were proposed by involving the momentum equation. However, these models were derived under ideal theoretical conditions and could require tremendous computation efforts in some cases. To solve them numerically within reasonable computational time, partial differential equations (PDE) are then used to discretize their model formulations, by the road segment and time period, into elements. In summary, such discrete reformulations can be classified into: the Godunov scheme (Lebacque, 1996), the upwind scheme (Lebacque et al., 2007), the Lax-Friedrichs scheme (Wong and Wong, 2002; Göttlich et al., 2013), and the Lax-Wendroff scheme (Michalopoulos et al., 1993). Cell transmission model (CTM) is one special case of Godunov scheme of the LWR where the Courant-Friedrichs-Lewy (CFL) number equals to 1 (Daganzo, 1994). To extend the PW model, Papageorgiou et al. (1989) proposed a discrete PW-like TSE model, METANET, and succeeded in reproducing complex traffic phenomena in a certain level. METANET has many successful applications in later studies. Hence, in view of the great computational efficiency of the discretized formulations, this study aims to investigate the numerical methods leveraging the discrete traffic flow models.

To calibrate the traffic flow model in real world applications, observations from stationary sensors (e.g.,

inductive loop, ultrasonic, radar, camera detectors) are usually leveraged and aggregated to average traffic flow and instant speed at a certain resolution. However, their accuracy and precision may be not reliable due to detection faults and uncertainties, such as frequent data missing and/or double counting of loop detectors (Chen et al., 2003b). To account for such data uncertainties, researchers developed stochastic traffic flow models (Gazis and Knapp, 1971; Szeto and Gazis, 1972; Gazis and Liu, 2003), which were performed by adding Gaussian noise terms to the model expressions and obtained real-world data were used to quantify those noises. As a stochastic adaption to the base model, the stochastic METANET is enhanced by adding flow and speed errors in the formulation and its parameters are estimated by Extended Kalman filter (EKF) (Wang and Papageorgiou, 2005; Wang et al., 2007). Notably, Kalman filter (KF) and its extensions are well-known data assimilation methods, including unscented Kalman filter (UKF) (Mihaylova et al., 2006), ensemble Kalman filter (EnKF) (Work et al., 2008), particle filter (PF) (Mihaylova and Boel, 2004), etc. However, it is pointed out in the literature that those simply-noised models could lead to the possibility of: (i) causing negative sample paths; (ii) producing mean dynamics that do not coincide with the original deterministic dynamics due to nonlinearity (Jabari and Liu, 2012); and (iii) propagating faster-than-vehicle speed information (Seo et al., 2017).

With the advances in data collecting and processing technologies, data-driven methods have been developed dramatically in recent years. This category of methods does not require explicit theoretical assumptions, such as fundamental diagrams and conservation law (Smith et al., 2003; Chen et al., 2003a). For example, machine learning (ML) models are prevailing in leveraging the voluminous data and capturing the stochasticity in TSE (Zhong et al., 2004; Ni and Leonard, 2005; Yin et al., 2012; Tang et al., 2015; Tak et al., 2016; Li et al., 2013; Tan et al., 2014, 2013; Duan et al., 2016; Polson and Sokolov, 2017b; Wu et al., 2018; Polson and Sokolov, 2017a). However, due to the data-driven nature, lack of the high-quality data would result in significant performance drops of ML models in the following scenarios: (i) training data are scarce and insufficient to reveal the complexity of the system; (ii) training data contain random noise, or include non-measurable incorrect/misleading information; and (iii) testing data are far from the training examples, i.e., extrapolation. Unfortunately, those scenarios commonly exist in practice due to the detection system and random errors, communication failure, and storage malfunction. Hence, when the data contain unignorable outliers, pure ML prediction will be biased due to the misleading training data. Although implementing a data screening and correction function before the ML training process could be helpful, in most cases, those incorrect data are not even able to be identified without further information (Lu et al., 2014).

Therefore, in view of the deficiencies of existing classical traffic flow models and pure ML models, hybrid methodologies which fuse capability of both offer a new alternative to address the TSE challenges. Among them, our pioneer work proposed the innovative Physics Regularized Machine Learning (PRML) framework to leverage the well-investigated theoretical formulations, such as fundamental diagrams and conservation law, to overcome the flawed data challenge in ML theories (Yuan et al., 2020). Compared with physics (i.e., macroscopic traffic flow) models, the PRML framework can capture the uncertainties in estimation which beyond the capability of closed-form expressions and eliminate the efforts in calibrating model parameters. In comparison to pure ML models, the PRML is more resistant to the data noise/ flaw as valuable knowledge from physics models can help regularize the learning process. Moreover, a PRML model is more explainable by learning parameters with physical meanings, and is expected to bridge the researches of classical traffic flow models and novel data-driven approaches.

As the current PRML theory (Wang et al., 2020; Yuan et al., 2020) can only adopt continuous physics

models, this study aims to advance this foundational theory to leverage both classical discrete macroscopic traffic flow models and data-driven methods. Compared with the continuous macroscopic traffic flow models (i.e. LWR, PW, ARZ models), the discrete macroscopic traffic flow models, i.e. METANET (Papageorgiou et al., 1989), may involve nondifferentiable discrete equations in spatial and temporal spaces. Although the current PRML framework is designed for physics models formulated in PDEs, it may also be applicable to nondifferentiable equations by similar encoding techniques. This study will adopt the Gaussian process as the ML component and extend the Physics Regularized Gaussian Process (PRGP) approach. More specifically, we focus on the key challenges of adopting discrete models: (a) migrating PDE encoding techniques to non-differentiable discrete equations as Gaussian processes, (b) implementing the Bayesian stochastic algorithm in auto-differentiation libraries, and (c) conducting a case study as well as a robust analysis regarding the data quality.

In summary, this paper contributes to the literature in the following aspects: 1) The PRGP framework overcomes the difficulty of including noisy data and non-measurable incorrect information in the ML training process; 2) The novel hybrid method can encode discrete traffic flow models into Gaussian processes and employs a Bayesian stochastic algorithm to estimate the model efficiently; 3) The proposed hybrid model brings transportation theoretical foundations to ML-based methodologies, makes the model more explainable (converts "black box" back to "white box"), while still keeps the advantage of data-driven approaches in capturing real-world uncertainties; and 4) Field stationary traffic detector data from a interstate freeway segment are utilized to justify the effectiveness and the applicability of the proposed method.

The remainder of this paper is organized as follows. Section 2 shows the classical discrete TSE modeling, its stochastic extensions and estimation methods. In Section 3, the integrated GP and physics model equations are formulated for encoding physical knowledge into Bayesian statistics, and the posterior regularized inference algorithm are presented in Section 4. In Section 5, the case study on a real-world data from the interstate freeway I-15 is conducted to justify the proposed methods. The conclusion section summarizes the critical findings and future research directions.

2. Fundamentals and Review of Macroscopic TSE Models

2.1. Notations and Variable Definitions

Similar to the existing literature, For the convenience of discussion, the following Table 1 summarizes key notations that have been used in the proposed PRGP model:

Table 1: List of Key Notations in the proposed PRGP Model

Notation	Definition
\mathcal{D}	the training data set;
d, d'	the dimension of the input and output, respectively;
f	the mapping from \mathbf{x} to \mathbf{y} ;
\mathbf{f}	the function value of the mapping f ;
$\hat{\mathbf{f}}$	the predicted function value;
g	the mapping from \mathbf{x} to the right-hand side of physical equations;
\mathbf{g}	the vector of the right-hand side of physical equations;
\mathbf{I}	the identity matrix;
I	the number of the highway segment;

i	the index of the highway segment;
j	the index of the observation in the data set;
K	the kernel function;
\mathbf{K}	the kernel value matrix regarding \mathbf{X} ;
$\hat{\mathbf{K}}$	the kernel value matrix regarding \mathbf{Z} ;
\mathbf{K}_*	the kernel value regarding \mathbf{X}^* ;
k	the index of the time step;
\mathcal{N}	the vectorized Gaussian distribution;
\mathbb{N}	the natural number set;
N	the number of segments on the highway;
n	the number of observations, in another word, the sample size;
m	the number of pseudo observations;
p	the index of the observation in the data set;
$q_{i,k}$	the total flow at the end of segment i ;
r_i	the inflow of vehicles at on-ramps;
s_i	the outflow of vehicles at off-ramps;
T	the time-discretization step;
t	the index of the algorithm iteration;
$v_{i,k}$	the average speed at segment i ;
v_f	the free-flow speed;
W	the total number of physics equations;
w	the index of physics equations;
\mathbf{X}	the data input vectors of size n ;
\mathbf{X}^*	separated input vectors for prediction;
\mathbf{x}	the model input vector, i.e. location, time;
\mathbf{Y}	the data output vectors of size n ;
\mathbf{y}	the model output vector, i.e. flow, speed, density;
\mathbf{Z}	the pseudo-observation input vector of size m ;
\mathbf{z}	the pseudo-observation input;
α	the exponent of the stationary speed equation;
$\beta_{i,k}$	the departure rate;
γ	the positive coefficient for the regularization effect;
Δ_i	the segment length at the segment;
ϵ	the Gaussian distributed random vector;
θ	all trainable parameters, including kernel parameters and model parameters;
$\rho_{i,k}$	the density at the end of segment i ;
ρ_{cr}	the critical density;
$\bar{\tau}$	the isotropic Gaussian noise level;
τ, ν, κ	positive physics model parameters;
$\xi_{i,k}^q$	the zero-mean Gaussian white noise acting on the empirical flow equation;
$\xi_{i,k}^v$	the zero-mean Gaussian white noise acting on the empirical speed equation;
μ, σ	the mean and standard deviation of the probability distribution;
η_1, η_2, η_3	kernel parameters;

2.2. Second order traffic flow model and its stochastic extensions

As an influential study in the literature, [Papageorgiou et al. \(1989\)](#) proposed a discrete macroscopic traffic flow model, METANET, which subdivided the highway sketch into N segments and considered the density $\rho_{i,k}$ of highway segment $i = 1, \dots, N$ at time step k to be the number of vehicles in the segment divided by the segment length Δ_i . The dynamics of the density can be described by Eq. 1.

$$\rho_{i,k+1} = \rho_{i,k} + \frac{T}{\Delta_i \lambda_i} [q_{i-1,k} - q_{i,k} + r_{i,k} - s_{i,k}] \quad (1)$$

The departure flow is assumed to be a portion of the flow at the segment in Eq. 2. It is assumed that any unmeasured on-ramp and off-ramp are constant, or, effectively, slowly varying so that the ramp flow may be captured by a random walk.

$$s_{i,k} = \beta_{i,k} \cdot q_{i-1,k} \quad (2)$$

The dynamics of the speed can be described by Eq. 3.

$$v_{i,k+1} = v_{i,k} + \frac{T}{\tau} [V(\rho_{i,k}) - v_{i,k}] + \frac{T}{\Delta_i} v_{i,k} (v_{i-1,k} - v_{i,k}) - \frac{\nu T}{\tau \Delta_i} \frac{\rho_{i+1,k} - \rho_{i,k}}{\rho_{i,k} + \kappa} - \frac{\delta T}{\Delta_i \lambda_i} \frac{r_{i,k} v_{i,k}}{\rho_{i,k} + \kappa} \quad (3)$$

The exponential fundamental diagram is shown in Eqs. 4-5.

$$V(\rho) = v_f \exp\left[-\frac{1}{\alpha} \left(\frac{\rho}{\rho_{cr}}\right)^\alpha\right] \quad (4)$$

$$q_{i,k} = \rho_{i,k} v_{i,k} \lambda_i \quad (5)$$

where Eqs. 1, 3, 4, 5 are the well-known conservation equation, dynamic speed equation, stationary speed equation, and flow equation, respectively; $\tau, \nu, \delta, \kappa, v_f, \rho_{cr}, \alpha$ are positive model parameters which are given the same values for all segments, specifically, v_f denotes the free-flow speed, ρ_{cr} the critical density, and α the exponent of the stationary speed equation. Considering the limitation of the METANET model in representing real-world traffic fluctuations, [Wang and Papageorgiou \(2005\)](#) added Gaussian error terms $\xi_{i,k}^v, \xi_{i,k}^q$ to the flow and speed equations (Eqs. 6-7) to capture the random errors of traffic detectors.

$$v_{i,k+1} = v_{i,k} + \frac{T}{\tau} [V(\rho_{i,k}) - v_{i,k}] + \frac{T}{\Delta_i} v_{i,k} (v_{i-1,k} - v_{i,k}) - \frac{\nu T}{\tau \Delta_i} \frac{\rho_{i+1,k} - \rho_{i,k}}{\rho_{i,k} + \kappa} - \frac{\delta T}{\Delta_i \lambda_i} \frac{r_{i,k} v_{i,k}}{\rho_{i,k} + \kappa} + \xi_{i,k}^v \quad (6)$$

$$q_{i,k} = \rho_{i,k} v_{i,k} \lambda_i + \xi_{i,k}^q \quad (7)$$

where $\xi_{i,k}^v, \xi_{i,k}^q$ denote zero-mean Gaussian white noise acting on the empirical equations and the approximate speed and flow equations, respectively, to reflect the modeling inaccuracies. Then an EKF function is implemented to dynamically correct the model estimates based on detector measurements. Notably, despite the successful applications and extensions, the EKF-based model may possibly produce infeasible behaviors, such as negative speed and information propagating faster-than-vehicle speed. This is due to the fact that nonlinear functions of Gaussian noise typically produce non-Gaussian and non-zero mean random noises ([Daganzo, 1995](#); [Del Castillo et al., 1994](#); [Hoogendoorn and Bovy, 2001](#); [Papageorgiou, 1998](#)). In the meantime, the calibration of model parameters and EKF initial covariance matrix, which often requires tremendous efforts, plays a key role in affecting TSE accuracy. In this study, METANET and its extended

version with EKF will both serve as benchmark models to evaluate the performance of the proposed PRGP model.

3. Formulation of the Physics Regularized Gaussian Process Model

To introduce the developed modeling framework of the physics regularized Gaussian process, this section reviews the key concept of the conventional Gaussian Process (GP) and its applications in the TSE problem, describes the modeling structure of the proposed PRGP, and illustrates how to encode the physical knowledge (i.e., traffic flow model), in a discretized formulation, into the GP framework.

3.1. Modeling framework

GP is a data-driven method for capturing the similarity between the system states, of which the core idea is to learn the kernel function (i.e. covariance) between variables and to predict the target by the linear combination of the training data (Rasmussen, 2003). Here, the main task of GP is to learn a mapping $\mathbf{f} : \mathbb{R}^d \rightarrow \mathbb{R}^{d'}$ from a d -dimensional space to a d' -dimensional space, based on a training set $\mathcal{D} = (\mathbf{X}, \mathbf{Y})$, where $\mathbf{X} = [\mathbf{x}_1, \dots, \mathbf{x}_n]^\top$ is the input vector, $\mathbf{Y} = [\mathbf{y}_1, \dots, \mathbf{y}_n]^\top$ is the output vector, \mathbf{x}_p is the d dimensional input vector, \mathbf{y}_p is the d' dimensional output vector, $\mathbf{f} = [f(\mathbf{x}_1), \dots, f(\mathbf{x}_n)]^\top$ is the learning function, and n refers to the sample size. The basic assumption is that the output \mathbf{Y} at the various input \mathbf{X} subjects to a multivariate GP with the covariance function of \mathbf{X} . Note that \mathbf{X}, \mathbf{Y} may have physical meanings only in their feasible domains. GP also assumes the noise in the data \mathbf{Y} . Given the data \mathbf{X}, \mathbf{Y} and the new input \mathbf{x}^* , the noise-free function value \mathbf{f} can be estimated based on Eq. 8.

$$p(\mathbf{f}(\mathbf{x}^*)|\mathbf{x}^*, \mathbf{X}, \mathbf{Y}) = \mathcal{N}(\mu(\mathbf{x}^*), \sigma(\mathbf{x}^*)) \quad (8)$$

where the mean $\mu(\mathbf{x}^*)$, standard deviation $\sigma(\mathbf{x}^*)$, and the kernel vector \mathbf{K}_* are calculated in Eqs. 9-11, respectively.

$$\mu(\mathbf{x}^*) = \mathbf{K}_*^\top (\mathbf{K} + \bar{\tau}^{-1} \mathbf{I})^{-1} \mathbf{Y} \quad (9)$$

$$\sigma(\mathbf{x}^*) = K(\mathbf{x}^*, \mathbf{x}^*) - \mathbf{K}_*^\top (\mathbf{K} + \bar{\tau}^{-1} \mathbf{I})^{-1} \mathbf{K}_* \quad (10)$$

$$\mathbf{K}_* = \left[K(\mathbf{x}^*, \mathbf{x}_1) \quad \dots \quad K(\mathbf{x}^*, \mathbf{x}_n) \right]^\top \quad (11)$$

The kernel K is defined as the non-parametric smooth positive-definite covariance function, such as the well-known Squared Exponential Automatic Relevance Determination (SEARD) Kernel and Radial Basis Function (RBF) kernel (Bishop, 2006). \mathbf{K} represents the kernel matrix, of which the elements are kernel values regarding the input \mathbf{X} . The employed kernel functions are shown as follows: The SE-ARD kernel is formulated in Eq. 12, where $\text{diag}(\cdot)$ represents the diagonal matrix, η_1 and η_2 are kernel parameters.

$$K(\mathbf{x}_p, \mathbf{x}_j) = \eta_1^2 \exp(-(\mathbf{x}_p - \mathbf{x}_j)^\top \text{diag}(\eta_2(\mathbf{x}_p - \mathbf{x}_j))) \quad (12)$$

The RBF kernel is formulated in Eq. 13, where η_3 is the kernel parameter.

$$K(\mathbf{x}_p, \mathbf{x}_j) = \exp\left(-\frac{(\|\mathbf{x}_p - \mathbf{x}_j\|)^2}{2\eta_3^2}\right) \quad (13)$$

For the application in the TSE problem, the designed concept of GP is illustrated in Fig. 2. The input \mathbf{x} represents the index of the segment and the time step, the output \mathbf{y} represents the corresponding vector

of flow, density, speed, as shown in Eqs. 14-15. Leveraging the GP, we can predict the unobserved traffic states in Eq. 18 from the samples in Eqs. 16-17.

$$\mathbf{x}_p = \begin{bmatrix} i & k \end{bmatrix}_{2 \times 1}^T \quad (14)$$

$$\mathbf{y}_p = \begin{bmatrix} q & \rho & v \end{bmatrix}_{3 \times 1}^T \quad (15)$$

$$\mathbf{X} = \begin{bmatrix} \mathbf{x}_1 & \mathbf{x}_2 & \cdots & \mathbf{x}_n \end{bmatrix}^T = \begin{bmatrix} i_1 & k_1 \\ i_2 & k_2 \\ \vdots & \vdots \\ i_n & k_n \end{bmatrix}_{n \times 2} \quad (16)$$

$$\mathbf{Y} = \begin{bmatrix} \mathbf{y}_1 & \mathbf{y}_2 & \cdots & \mathbf{y}_n \end{bmatrix}^T = \begin{bmatrix} q_1 & \rho_1 & v_1 \\ q_2 & \rho_2 & v_2 \\ \vdots & \vdots & \vdots \\ q_n & \rho_n & v_n \end{bmatrix}_{n \times 3} \quad (17)$$

$$\hat{\mathbf{f}} = \begin{bmatrix} \mu^{(q)}(\mathbf{x}) & \mu^{(\rho)}(\mathbf{x}) & \mu^{(v)}(\mathbf{x}) \end{bmatrix}_{3 \times 1}^T \quad (18)$$

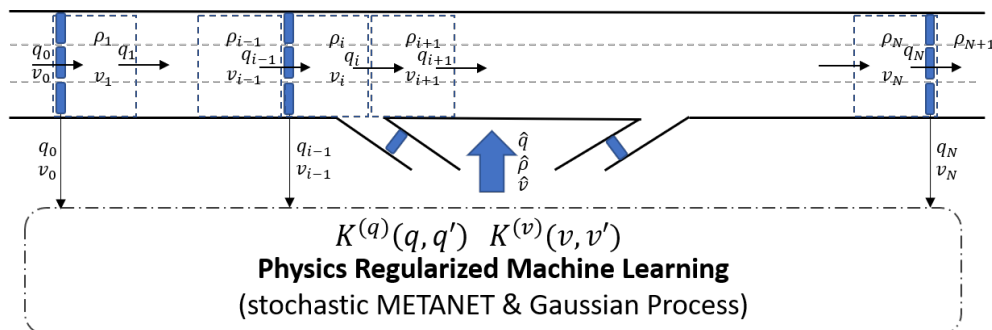


Figure 2: The proposed framework for physics regularized Gaussian process learning

However, it should be noted that GP heavily relies on data quality and its produced results are usually hard to interpret with physical meanings. This is also commonly recognized as a critical limitation of pure data-driven approaches and many ML models suffer from the same deficiency. To address this issue, the proposed PRGP employs the valuable physical knowledge, from the classical traffic flow models, to regularize the training process for more robust and explainable performances. Fig. 3 compares the concepts of pure GP and the proposed PRGP by depicting the observed traffic state, the GP predicted traffic state, and the PRGP predicted traffic state in three rectangles, where the blue square are for noisy observed states, pink squares represents biased observations, white squares represents the unobserved states, and green squares are for the predicted states. In the real-world cases, the raw data may be biased, noisy and missing due to system and communication failure, etc. Note that the flow, density and speed do not have physical meanings and are only separated isotropic dimensions in the pure GP framework. To repair the data-based flaw, the proposed PRGP leverages the *a priori* dynamics between the traffic state measures for improving the prediction accuracy and robustness.

In the proposed framework, the physical knowledge (i.e. traffic flow models) is encoded into GPs, which

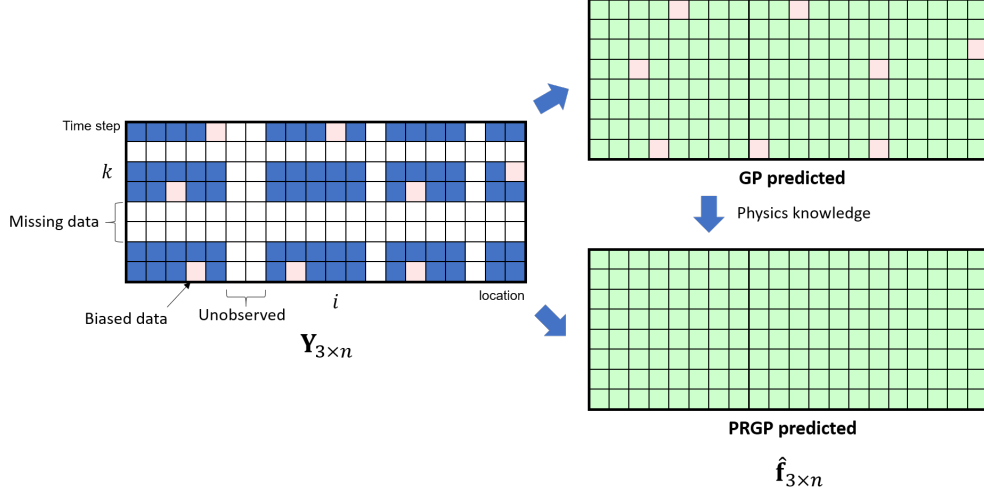


Figure 3: Conceptual comparison between PRGP and GP

captures both the stochasticity due to flawed/noisy data as well as the unobserved factors, such as missing on-ramp or off-ramp data.

3.2. Encoding the traffic flow model

In this section, we present the procedure to encode the traffic flow model into Gaussian process, under the stochastic framework. Fig. 4 shows how to reformulate the physics equations (the traffic flow model) into a generative component for regularization, where the nodes represents GPs; the arrows represents the stochastic conditional dependency between GPs; and the equations above the arrows show the computational transition from one GP to another.

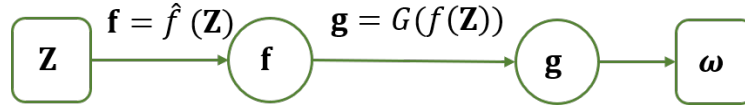


Figure 4: Encoding physics equations into Gaussian process

In Fig. 4, the input vector \mathbf{Z} with the length of m is given in Eq. 19. For the convenience of computation, we further introduce a set of m pseudo observations, $\omega = [0, \dots, 0]^\top$, as dummy outputs. The pseudo observation pair \mathbf{Z}, ω has the same structure with the data observation pair \mathbf{X}, \mathbf{Y} , and is designed to encode the physics equations into GP.

$$\mathbf{Z} = [\mathbf{z}_1, \dots, \mathbf{z}_m]^\top = \begin{bmatrix} i_1 & k_1 \\ i_2 & k_2 \\ \vdots & \vdots \\ i_m & k_m \end{bmatrix}_{2 \times m} \quad (19)$$

The physics equations are supposed to be in form of Eq. 20, where $\hat{\mathbf{f}}(\mathbf{Z})$ is the predicted outputs upon the input \mathbf{Z} and $\mathbf{G}[\cdot]$ is a physics model function of the output. The physics equations are converted into the desired function forms by moving terms to one side of equation and let the other side be zero. Then, when the data perfectly meets with the physics model function, the remaining error \mathbf{g} is supposed to be close to

zero. Considering the unobserved latent value and the data error, \mathbf{g} is assumed to be a GP.

$$\mathbf{G}[\hat{\mathbf{f}}(\mathbf{Z})] = \mathbf{g} \quad (20)$$

In the METANET model, the physics equations are related to four neighboring inputs, $\mathbf{Z}_{0,0}, \mathbf{Z}_{0,1}, \mathbf{Z}_{-1,0}$, and $\mathbf{Z}_{1,0}$, in time and space, and the corresponding outputs, $\mathbf{f}(\mathbf{Z}_{0,0}), \mathbf{f}(\mathbf{Z}_{0,1}), \mathbf{f}(\mathbf{Z}_{-1,0}), \mathbf{f}(\mathbf{Z}_{1,0})$, are predicted for yielding the resultant right-hand-side value \mathbf{g} in Eq. 21, where the subscript refers to the difference in elements of the input vector $\mathbf{z} = [i, k]$. For example, if the element in the input matrix $\mathbf{Z}_{0,0}$ is $[i, k]$, the corresponding element in $\mathbf{Z}_{0,1}$ is $[i, k + 1]$. Eq. 22 shows the equivalent formation of Eq. 21, where each row of the equation corresponds to Eqs. 23-25, respectively.

$$\mathbf{G}[\mathbf{f}(\mathbf{Z}_{0,0}), \mathbf{f}(\mathbf{Z}_{0,1}), \mathbf{f}(\mathbf{Z}_{-1,0}), \mathbf{f}(\mathbf{Z}_{1,0})] = \mathbf{g} \quad (21)$$

$$\begin{bmatrix} G_1 \left[\begin{array}{ccc} \mathbf{f}(\mathbf{Z}_{0,0}) & \mathbf{f}(\mathbf{Z}_{0,1}) & \mathbf{f}(\mathbf{Z}_{-1,0}) \\ \mathbf{f}(\mathbf{Z}_{0,0}) & \mathbf{f}(\mathbf{Z}_{0,1}) & \mathbf{f}(\mathbf{Z}_{-1,0}) & \mathbf{f}(\mathbf{Z}_{1,0}) \\ \mathbf{f}(\mathbf{Z}_{0,0}) \end{array} \right] \\ G_2 \left[\begin{array}{ccc} \mathbf{f}(\mathbf{Z}_{0,0}) & \mathbf{f}(\mathbf{Z}_{0,1}) & \mathbf{f}(\mathbf{Z}_{-1,0}) & \mathbf{f}(\mathbf{Z}_{1,0}) \\ \mathbf{f}(\mathbf{Z}_{0,0}) \end{array} \right] \\ G_3 \left[\begin{array}{c} \mathbf{f}(\mathbf{Z}_{0,0}) \end{array} \right] \end{bmatrix} = \begin{bmatrix} g_1 \\ g_2 \\ g_3 \end{bmatrix} \quad (22)$$

The traffic flow model METANET is reformulated to the functions of predictions in Eqs. 23-25. The encoded physics equations do not have to be the exactly same formulations. Note that the on-ramp off-ramp flows, $r_{i,k}, s_{i,k}$, are assumed to be not observed, and are removed in Eq. 23, and the unobserved measures and noise are captured by the right-hand side term g_1 . In the test, a small number is also added to the denominators in Eqs. 23-25 to prevent the numerical problem.

$$G_1(\hat{\mathbf{f}}) = \hat{\rho}_{i,k+1} - \hat{\rho}_{i,k} - \frac{T}{\Delta_i \lambda_i} [\hat{q}_{i-1,k} - \hat{q}_{i,k}] = g_1 \quad (23)$$

$$G_2(\hat{\mathbf{f}}) = \hat{v}_{i,k+1} - \hat{v}_{i,k} + \frac{T}{\tau} [V(\hat{\rho}_{i,k}) - \hat{v}_{i,k}] - \frac{T}{\Delta_i} \hat{v}_{i,k} (\hat{v}_{i-1,k} - \hat{v}_{i,k}) + \frac{\sigma T}{\tau \Delta_i} \frac{\hat{\rho}_{i+1,k} - \hat{\rho}_{i,k}}{\hat{\rho}_{i,k} + \kappa} = g_2 \quad (24)$$

$$G_3(\hat{\mathbf{f}}) = \hat{q}_{i,k} - \hat{\rho}_{i,k} \hat{v}_{i,k} \lambda_i = g_3 \quad (25)$$

To enable Bayesian framework that incorporates the physical knowledge, we propose a generative component $p(\omega|\mathbf{X}, \mathbf{Y})$ that acts as a regularizer on the GP model $p(\mathbf{Y}|\mathbf{X})$. To sample the pseudo observation ω , we sample the posterior function values at each $\mathbf{z}_j, j = 1, \dots, m$ from a Gaussian distribution as shown in Eq. 26. It can also be noted that Eq. 26 has the same form as Eq. 8 at input values \mathbf{Z} .

$$p(f(\mathbf{z}_j)|\mathbf{z}_j, \mathbf{X}, \mathbf{Y}) = \mathcal{N}(\mu(\mathbf{z}_j), \sigma(\mathbf{z}_j)), \forall j = 1, \dots, m \quad (26)$$

Then we will obtain the predicted physical function values at \mathbf{Z} , $\mathbf{g} = [g(\mathbf{z}_1), \dots, g(\mathbf{z}_m)]^\top$. Given the remainder value vector \mathbf{g} of the physics equations, we sample the pseudo observations ω from another GP. The predicted output $f(z)$ is substituted to the physics model to yield the right-hand side values \mathbf{g} .

$$p(\omega|\mathbf{g}, \mathbf{Z}) = \mathcal{N}(\mathbf{g}, \hat{\mathbf{K}}) \quad (27)$$

where $\hat{\mathbf{K}}$ is the covariance matrix of the shadow GP and each element is calculated from the kernel $\hat{K}(\cdot, \cdot)$, as shown in Eq. 28.

$$\hat{\mathbf{K}} = \begin{bmatrix} \hat{K}(\mathbf{x}_1, \mathbf{z}_1) & \cdots & \hat{K}(\mathbf{z}_1, \mathbf{z}_j) & \cdots & \hat{K}(\mathbf{z}_1, \mathbf{z}_m) \\ \vdots & & \vdots & & \vdots \\ \hat{K}(\mathbf{x}_i, \mathbf{z}_1) & \cdots & \hat{K}(\mathbf{x}_i, \mathbf{z}_j) & \cdots & \hat{K}(\mathbf{x}_i, \mathbf{z}_m) \\ \vdots & & \vdots & \ddots & \vdots \\ \hat{K}(\mathbf{x}_n, \mathbf{z}_1) & \cdots & \hat{K}(\mathbf{x}_n, \mathbf{z}_j) & \cdots & \hat{K}(\mathbf{x}_n, \mathbf{z}_m) \end{bmatrix} \quad (28)$$

Considering the symmetry property of the Gaussian distribution, as shown in Eq. 29, the sampling of the pseudo observations in essence is equivalent to placing another GP prior over the sampled physics equation \mathbf{g} . Therefore, this GP prior regularizes the sampled function. If the likelihood is maximized of both the original GP and the generative component, the parameters of the original GP are regularized by the equations of the physics model.

$$p(\omega|\mathbf{g}, \hat{\mathbf{K}}) = p(\mathbf{g}|\omega, \hat{\mathbf{K}}) = p(\hat{\mathbf{f}}(\mathbf{z})|\omega, \hat{\mathbf{K}}) \quad (29)$$

Thus, given a dataset $\{\mathbf{X}, \mathbf{Y}\}$, the joint probability of the generative component $p(\omega, \mathbf{g}, \hat{\mathbf{f}}, \mathbf{Z}|\mathbf{X}, \mathbf{Y})$ is broken into four parts, as shown in Eq. 30.

$$p(\omega, \mathbf{g}, \hat{\mathbf{f}}, \mathbf{Z}|\mathbf{X}, \mathbf{Y}) = p(\mathbf{Z})p(\hat{\mathbf{f}}|\mathbf{Z}, \mathbf{X}, \mathbf{Y})p(\mathbf{g}|\hat{\mathbf{f}})p(\omega|\mathbf{g}) \quad (30)$$

where the prior of the m inputs, $p(\mathbf{Z})$, $p(\hat{\mathbf{f}}|\mathbf{Z}, \mathbf{X}, \mathbf{Y})$, and $p(\omega|\mathbf{g})$ are formulated in Eqs. 31-33, respectively. Note that when no extra knowledge is available, \mathbf{z}_j can be randomized from uniform distribution assumedly. To predict the GP values $\hat{\mathbf{f}}$, the critical task is to estimate the kernel functions $\mathbf{K}, \hat{\mathbf{K}}$. By assuming the kernel functions $\mathbf{K}, \hat{\mathbf{K}}$ have the formulations in Eq. 12-13, the hyperparameters of the kernel functions are to be estimated by training on the dataset. Given the learned hyperparameters of the kernel functions, the predicted outputs $\hat{\mathbf{f}}$ is calculated by Eqs. 8-Eq. 11.

$$p(\mathbf{Z}) = \prod_{j=1}^m p(\mathbf{z}_j) \quad (31)$$

$$p(\hat{\mathbf{f}}|\mathbf{Z}, \mathbf{X}, \mathbf{Y}) = \prod_{j=1}^m [\mathcal{N}(\hat{\mathbf{f}}(\mathbf{z}_j)|\mu(\mathbf{z}_j), \sigma(\mathbf{z}_j))] \quad (32)$$

$$p(\omega|\mathbf{g}) = \mathcal{N}(\mathbf{g}, \hat{\mathbf{K}}) \quad (33)$$

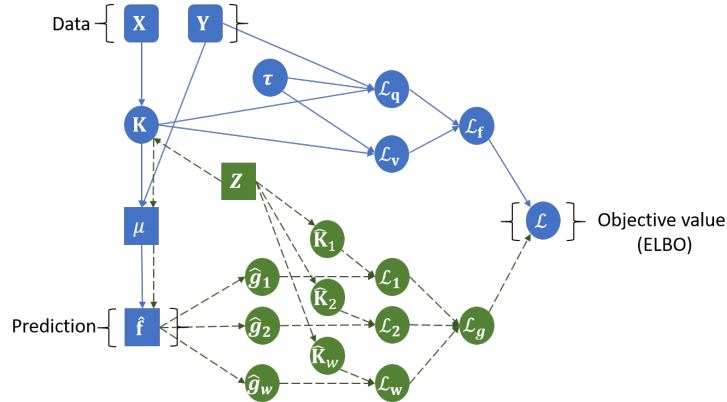


Figure 5: The computational graph of the prediction and the loss function

To illustrate the structure of the proposed PRGP method, Fig. 5 depicts the computational graph, where the vertices represent for the variables (i.e. scalars, matrices, or tensors), the circle vertices involve trainable parameters, the squared vertices represents the prediction, the rounded rectangles are for the data set; the arrows represent the equation calculation; the blue vertices and arrows are for the original GP, and the green vertices are for the physics regularizer. The computational graph shows the computational dependency of the variables so that each vertex is computed from a function of precursive variables. Given the computational graph, the auto-differentiation libraries can find the gradient of the loss function for optimizing the trainable parameters iteratively.

4. Solution Algorithm

Posterior regularization is a powerful inference methodology in the Bayesian stochastic modeling framework (Ganchev et al., 2010). A variety of successful posterior regularization algorithms have been proposed (He et al., 2013; Ganchev and Das, 2013; Zhu et al., 2014; Libbrecht et al., 2015; Song et al., 2016). The posterior regularization is based on optimizing the parameters to maximize the likelihood or the evidence lowerbound (ELBO) of the likelihood. The objective includes the model likelihood on data and a penalty term that encodes the constrains over the posterior of the variables. Via the penalty term, we can incorporate our domain knowledge or constrains outright to the posteriors, rather than through the priors and a complex, intermediate computing procedure. Fig. 6 depicts one iteration in the high dimensional parameter space to illustrate the design concept of the proposed posterior regularization algorithm for the proposed model. In Fig. 6, the parameter space consists of the two dimensions of the outputs (i.e. flow and speed q, v); the dots show the vector of parameters $\theta^{(t)}$ is updated to the new vector $\theta^{(t+1)}$ via the auto-differentiation in the t^{th} iteration; the arrows show the directions of the gradients of the loss function (i.e. evidence lowerbound of likelihood); the blue arrows represent the increments via the conventional GP in two dimensions, the green arrow shows the increment via the proposed physical knowledge regularizer, and the red arrow is the resultant sum of increments.

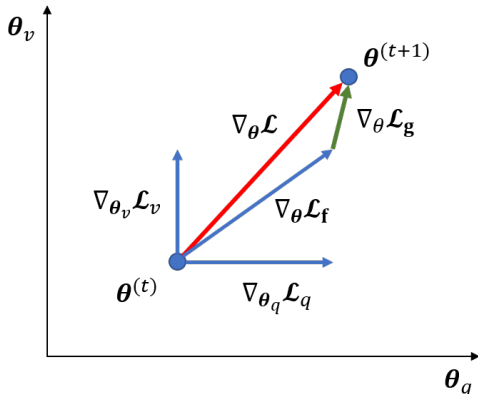


Figure 6: The posterior regularization algorithm for the proposed model

The sum of the evidence lowerbound of likelihoods across the GP and the physical knowledge GP, \mathcal{L} and the proposed inference algorithm are derived as follows. For convenient effective efficient model inference, we marginalize out all variables in the joint probability to avoid estimating extra approximate posteriors. Then we derive a convenient evidence lower bound to enable the linear transformation. Using the auto-

differentiation libraries, we develop an efficient stochastic optimization algorithm based on the posterior regularization inference framework.

The generative component in Eq. 30 is bind to the conventional GP to obtain a new principled Bayesian model. The joint probability of the stochastic model is given by Eq. 34. In last section, the joint probability $p(\omega, \mathbf{g}, \hat{\mathbf{f}}, \mathbf{Z}|\mathbf{X}, \mathbf{Y})$ is derived in Eqs. 30-33.

$$p(\mathbf{Y}, \omega, \mathbf{g}, \hat{\mathbf{f}}, \mathbf{Z}|\mathbf{X}) = p(\mathbf{Y}|\mathbf{X})p(\omega, \mathbf{g}, \hat{\mathbf{f}}, \mathbf{Z}|\mathbf{X}, \mathbf{Y}) \quad (34)$$

In this section, we derive the objective function and propose an iterative algorithm to solve the problem. We first marginalize out all the variables in the generative component to avoid approximating their posterior in Eq. 35.

$$\begin{aligned} p(\omega|\mathbf{X}, \mathbf{Y}) &= \iiint [p(\omega, \mathbf{g}, \hat{\mathbf{f}}, \mathbf{Z}|\mathbf{X}, \mathbf{Y})d\mathbf{Z}d\mathbf{g}d\hat{\mathbf{f}}] \\ &= \mathbb{E}_{p(\mathbf{Z})}\mathbb{E}_{p(\hat{\mathbf{f}}|\mathbf{Z}, \mathbf{X}, \mathbf{Y})}\mathcal{N}(\Psi\hat{\mathbf{f}}|\mathbf{0}, \hat{\mathbf{K}}) \end{aligned} \quad (35)$$

The prefixed positive parameter γ is used to control the strength of regularization effect. The larger the value of γ , the greater regularization effect we apply on the learning process.

$$p(\mathbf{Y}, \omega|\mathbf{X}) = p(\mathbf{Y}|\mathbf{X})p(\omega|\mathbf{X}, \mathbf{Y})^\gamma \quad (36)$$

The objective is to maximize the log-likelihood in Eq. 37. However, the log-likelihood is intractable due to the expectation inside the logarithm term. To address this problem, the Jensen's inequality is used to obtain the evidence lower bound (ELBO) \mathcal{L} .

$$\begin{aligned} \log[p(\mathbf{Y}, \omega|\mathbf{X})] &= \log[p(\mathbf{Y}|\mathbf{X})] + \gamma \log[p(\omega|\mathbf{X}, \mathbf{Y})] \\ &= \log[\mathcal{N}(\mathbf{Y}|\mathbf{0}, \hat{\mathbf{K}} + \tau^{-1}\mathbf{I})] \\ &\quad + \gamma \log[\mathbb{E}_{p(\mathbf{Z})}\mathbb{E}_{p(\hat{\mathbf{f}}|\mathbf{Z}, \mathbf{X}, \mathbf{Y})}[\mathcal{N}(\Psi\hat{\mathbf{f}}|\mathbf{0}, \hat{\mathbf{K}})]] \\ &\geq \mathcal{L} = \log[\mathcal{N}(\mathbf{Y}|\omega, \hat{\mathbf{K}} + \tau^{-1}\mathbf{I})] \\ &\quad + \gamma \mathbb{E}_{p(\mathbf{Z})}\mathbb{E}_{p(\hat{\mathbf{f}}|\mathbf{Z}, \mathbf{X}, \mathbf{Y})}[\log[\mathcal{N}(\Psi\hat{\mathbf{f}}|\omega, \hat{\mathbf{K}})]] \end{aligned} \quad (37)$$

The log-likelihood and the ELBO of the traffic flow model can be formulated in Eq. 38.

$$\begin{aligned} \log[p(\mathbf{Y}, \omega|\mathbf{X})] \geq \mathcal{L} &= \sum_{i=1}^{d'} \log[\mathcal{N}([\mathbf{Y}]_i|\omega, \hat{\mathbf{K}}_i + \tau^{-1}\mathbf{I})] \\ &\quad + \sum_{w=1}^W \gamma_w \mathbb{E}_{p(\mathbf{z})}\mathbb{E}_{p(\hat{\mathbf{f}}_w|\mathbf{z}, \mathbf{X}, \mathbf{Y})}[\log[\mathcal{N}(\Psi\hat{\mathbf{f}}_w|\omega, \hat{\mathbf{K}}_w)]] \end{aligned} \quad (38)$$

The parameter θ is defined in Eq. 39.

$$\theta = [\theta_f \quad \theta_g]^\top = [\bar{\tau} \quad \eta \quad \tau \quad \nu \quad \delta \quad \kappa \quad v_f \quad \rho_{cr} \quad \alpha \quad \dots]^\top \quad (39)$$

Thus, we can obtain the ELBO of the log-likelihood in Eq. 37 by maximizing \mathcal{L} via stochastic optimization as shown in Alg. 4, where ϕ refers to the learning rate and θ denotes all trainable parameters.

- 1: Initialization
- 2: **while** not reach stopping criteria **do**
- 3: Sample a set of input locations \mathbf{Z}
- 4: Estimate the posterior target function values $\mathbf{f}(\hat{\mathbf{Z}}) = \mathbf{K}_*^\top (\mathbf{K} + \bar{\tau}^{-1} \mathbf{I})^{-1} \mathbf{Y}$
- 5: Calculate ELBO $\tilde{\mathcal{L}} = [\tilde{\mathcal{L}}_f, \tilde{\mathcal{L}}_g]^\top$ with samples $(\mathbf{X}, \mathbf{Y}), (\mathbf{Z}, \hat{\mathbf{f}})$
- 6: Derive the gradients $\nabla_\theta \tilde{\mathcal{L}}$ and update the parameters $\theta^{(t+1)} = \theta^{(t)} + \phi \nabla_\theta \tilde{\mathcal{L}}$ via the unconstrained nonlinear optimization technique
- 7: **end while**
- 8: Output learned parameters θ

5. Numerical Examples and Model Evaluations

5.1. Data Collection and Case Setup

To evaluate the performance of the proposed method, we applied the PRGP method to estimate the traffic flow in a stretch of the interstate freeway I-15 across Utah, U.S. The Utah Department of Transportation (UDOT) has installed sensors every a few miles along the freeway. Each sensor counts the number of vehicles passed every minute, measures the speed of each vehicle, and sends the data back to a central database, called Performance Measurement System (PeMS). The collected real-time data and road conditions are available online and can be accessed by the public.

To prove the superiority of the proposed PRGP compared with the pure ML method and the physics models, this section aims to compare the proposed PRGP method with calibrated deterministic baseline model (Papageorgiou et al., 1989), the Extended Kalman filter (EKF) on the stochastic model (Wang and Papageorgiou, 2005), and pure Gaussian Process model. The parameters of the key notations of the METANET and EKF have been calibrated with the field data. The studied stretch is illustrated in Fig. 7, where the blue bars represent the locations of traffic detectors.

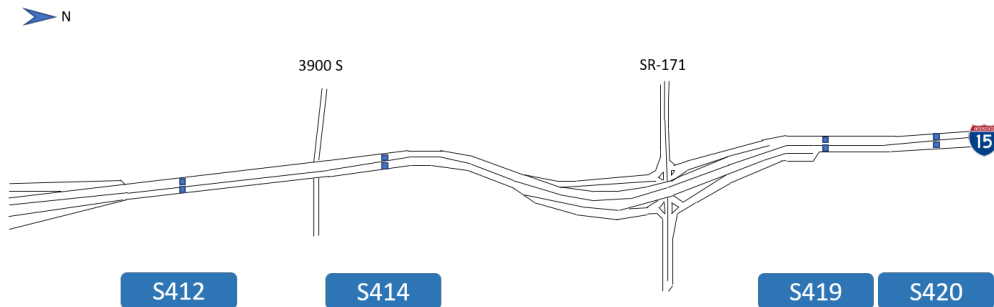


Figure 7: The stretch of the studied freeway segment which includes 4 detectors

The input variables include the location mileage of each sensor and the time of each read. In the literature, the data index representation (\mathbf{X}, \mathbf{Y}) has three major variations: (road segment, time interval), (road segment, day, time interval) and (road segment, week, day-of-week, time interval). In the experiments, we use the compatible representation (road segment, time interval), namely (i, k) , for consistence purpose. The traffic measures, flow q and speed v , are employed in the training and testing because the density is directly related to these two measures and is not recorded in the original data source. Note that the other variations of structural representation of the data are fully compatible with the proposed framework, and the impact of the data representation may depend on the specific case. Various data spans in spatial

and temporal dimensions are tested. In the studied scenario, the separate freeway segment in I-15 has 4 detectors. The data was collected from August 5, 2019 to August 19, 2019. Since the data is collected every 5 *min*, there are 288 observations per detector per day.

To further test the robustness of methods in each case, we investigate the biased data scenarios by artificially adding high measure biases to the traffic flow in the training data to mimic the common device malfunction situations. The robustness analysis is conducted to show the capability of dealing with the unpredictable misleading inputs in the training phase. Theoretically, the proposed PRGP is more robust than pure GP on noisy dataset. To justify this feature, a certain portion of the training dataset is replaced by synthesized noise. The testing set is not polluted original data. However, it should be noted that the comparable methods, offline METANET method and EKF, for METANET are not designed to contend the biased data.

In the setup of the experiments, the prefixed parameters of the proposed method are summarized in Table 2. Note that the strength of regularization λ does not need to be fine-tuned because the gradients of the parts of the loss function can be yield separately regarding the parameters.

Table 2: The prefixed parameters of the proposed method

Parameter	Value
Training set size	2880
Testing set size	576
The number of pseudo observations m	10
The number of iterations	500
The learning rate ϕ	0.01
The number of physics equations	3

The parameters of the calibrated models are listed as follows. Table 3 shows the initial METANET model parameters and the parameters for EKF are listed in Table 4.

Table 3: The initial parameters of the physical model

Parameter	Value (unit)
I	10
N	20
T	1/360 (<i>h</i>)
v_f	120 (<i>km/h</i>)
ν	35 (<i>km²/h</i>)
δ	1.4
τ	0.05 (<i>h</i>)
α	1.4324
Δ_i	0.5 (<i>km</i>)
ρ_{cr}	36.85 (<i>veh/km</i>)
κ	13 (<i>veh/lm</i>)
λ_i	4

The proposed inference algorithm is implemented in the open-source auto-differentiable computational graph framework, *Tensorflow*, where the optimizer ADAM (Kingma and Ba, 2014) is chosen for updating the parameters by rule-of-thumb. Note that the implementation of the proposed method does not rely on the specific framework, and the comparable libraries are potentially feasible as well. The computational

Table 4: The initial parameters of Extended Kalman filter

Parameter	Value (unit)
$D(\xi_{i,k}^q)$	100 <i>veh/h</i>
$D(\xi_{i,k}^v)$	11 <i>km/h</i>
$D(\xi_{0,k}^q)$	100 <i>veh/h</i>
$D(\xi_{0,k}^v)$	5 <i>km/h</i>
$D(\xi_{11,k}^\rho)$	1.5 <i>veh/km/lane</i>
$D(\xi_{\Gamma,k}^\Gamma)$	3 <i>veh/h</i>
$D(\xi_{9,k}^\beta)$	0.001
$D(\gamma_{i,k}^q)$	100 <i>veh/h</i>
$D(\gamma_{i,k}^v)$	10 <i>km/h</i>
$D(\gamma_{\Gamma,k}^\Gamma)$	20 <i>veh/h</i>
$D(\gamma_{9,k}^s)$	10 <i>veh/h</i>
$D(\xi_k^{uf})$	0.5 <i>veh/h</i>
$D(\xi_k^{cr})$	0.1 <i>veh/km/lane</i>
$D(\xi_k^a)$	0.01

complexity is cubic of the product of the sample size and the output dimension $O((Nd')^3 + m^3)$. In the experiments, the program costs 8,480 seconds on average on a workstation equipped with a 3.5GHz 6-core CPU. In the testing phase, the time complexity of the model estimation is marginal (less than 1 second) empirically, similar to all ML models. Note that the computational process can be accelerated by about 5 time if a NVIDIA CUDA-capable GPU is used. To quantify the precision of outputs, Rooted Mean Squared Error (RMSE) and Mean Absolute Percentage Error (MAPE) of each dimension are used as the performance metric, which are defined in Eqs. 40-41.

$$RMSE_j = \sqrt{\frac{1}{n} \sum_{i=1}^n \left(\frac{[\mathbf{y}_j]_i - [\hat{\mathbf{f}}_j]_i}{\sigma_i} \right)^2}, \forall j \in 1, \dots, d' \quad (40)$$

$$MAPE_j = \frac{100\%}{n} \sum_{i=1}^n \left| \frac{[\mathbf{y}_j]_i - [\hat{\mathbf{f}}_j]_i}{[\mathbf{y}_j]_i} \right|, \forall j \in 1, \dots, d' \quad (41)$$

The testing cases are constructed in two categories: (I) unobserved locations, and (II) random missing data. Note that Case I is the common scenario for TSE problems and the model-based data assimilation methods are compatible with Case I. Case II is for the data imputation task and is not of a fair comparison since the baseline method is not capable to impute missing data and would consequently perform disappointingly bad. The number of unobserved locations (i.e. no detector for training) is set to 2 in all cases. The missing data rate is 0.66. The data imputation methods are designed to contend the Case II. Fig. 8 depicts the data set used in the training and testing.

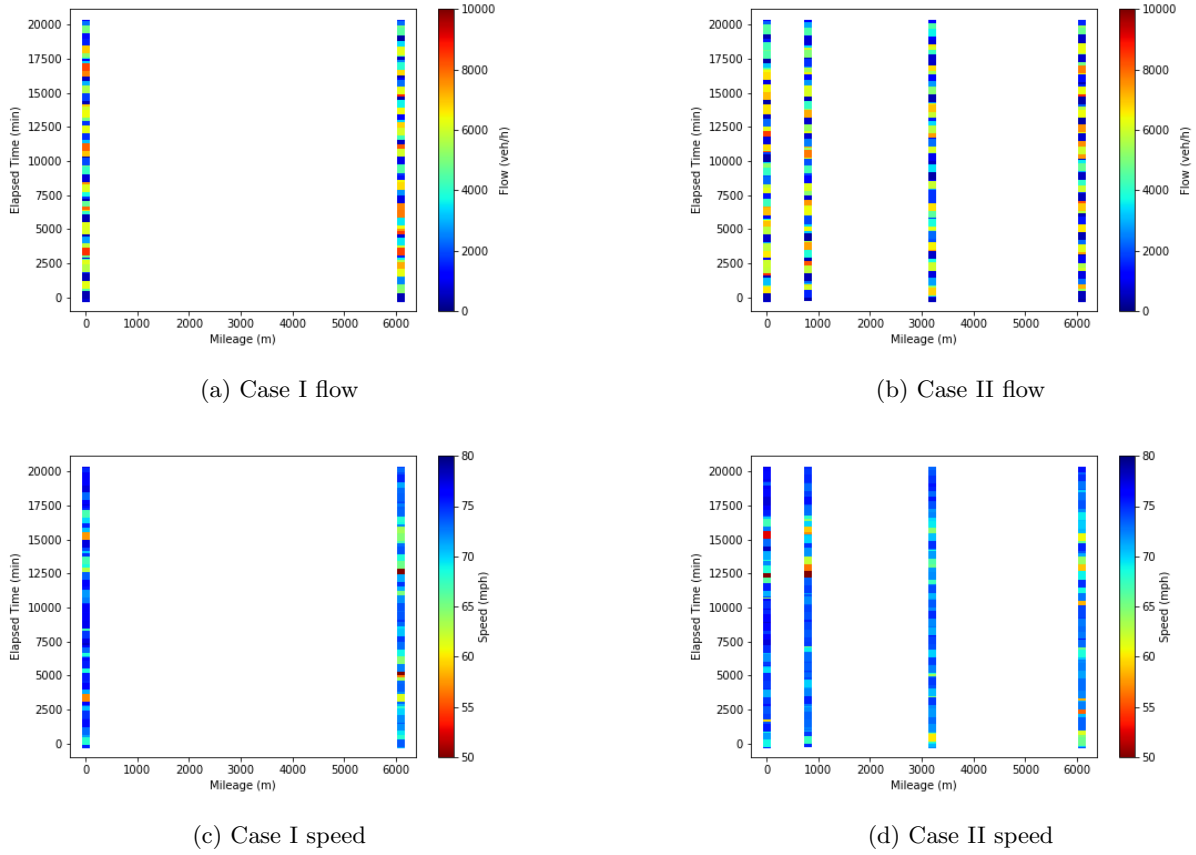


Figure 8: Sample data in the studied cases

5.2. Numerical studies with Case I

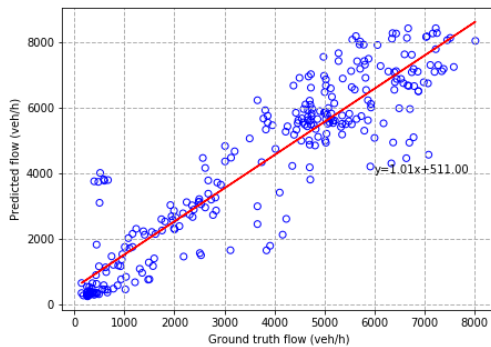
5.2.1. Results Analysis

Table 5 shows the results of the proposed method and the physics-based methods, where the method METANET represents the off-line calibrated fixed parameter METANET model, the METANET-EKF refers to the extended Kalman filter for online correcting the parameters of METANET model, pure GP means the Gaussian process based pure machine learning method, and PRGP refers to the proposed physics regularized Gaussian process with the aid of METANET. In comparison to the physics models, the GP can obviously outperform the physics models in terms of providing more accurate estimations of both flows and speeds. The GP can yield a $77.18 \text{ veh}/5\text{min}$ of RMSE and a 27.40% of MAPE for flow and a 5.19 mph of RMSE and a 4.74% for MAPE for speed, while the physics model based methods produced much higher RMSEs and MAPEs of both flow and speed estimates. Further comparison between the pure GP and the PRGP models reveal that PRGP models can improve the accuracy of both flow and speed estimations. However, the improvement is not significant, which is because pure GP can already achieve a very good estimation performance and leaves limited space for improvement by the PRGP. Note that the inputs of the proposed PRGP-based methods and classical traffic flow models are different. The latter method often requires the on-ramp and off-ramp flow observations as inputs, while the proposed method assumes unobserved on-ramp and off-ramp flows in the framework and does not require such data. Fig. 9 and Fig. 10 compare the flow and speed estimation and the ground truth for the Case I, respectively. In each figure, the blue dot shows the estimated value versus the ground true value, and if the slope of the red trend line is closed to 1 and the intercept is closed to 0, the estimation result is considered to be accurate. Fig 9 shows

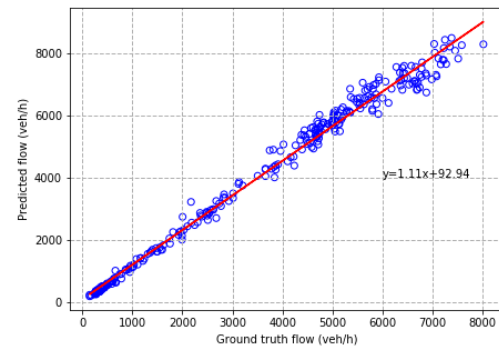
the METANET-EKF method outperforms the METANET in flow prediction, however, both of them have lower accuracy in speed prediction than GP and PRGP. The proposed PRGP has similar flow accuracy as GP, and slightly better speed accuracy than GP.

Table 5: Comparison of the results of the proposed method and the physics-based methods in Case I

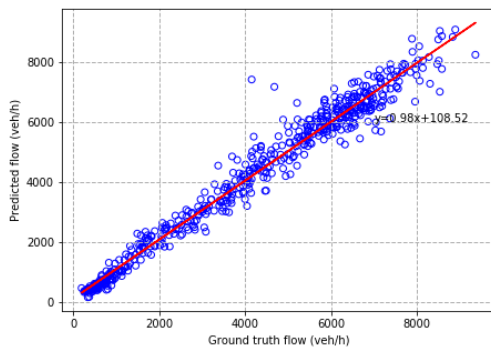
Method	RMSE of flow (veh/5min)	MAPE of flow	RMSE of speed (mph)	MAPE of speed
METANET	96.17	37.48%	9.11	11.4%
METANET-EKF	82.48	35.95%	5.74	7.17%
pure GP	77.18	27.40%	5.19	4.79%
PRGP	75.83	25.43%	5.09	4.60%



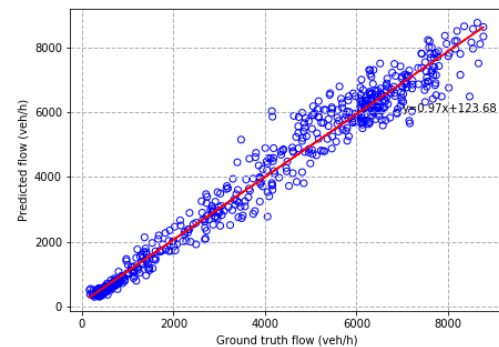
(a) METANET



(b) METANET-EKF



(c) GP

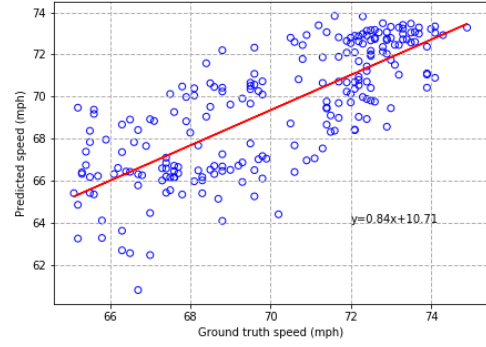


(d) PRGP-METANET

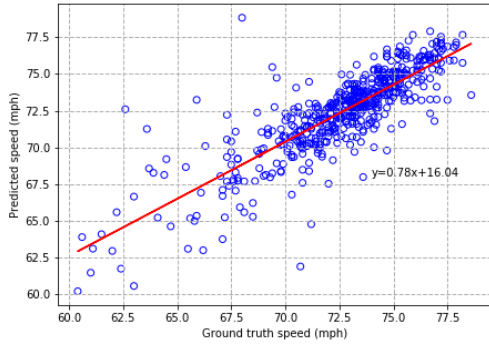
Figure 9: Comparison between flow estimations and the ground truth under missing data in Case I



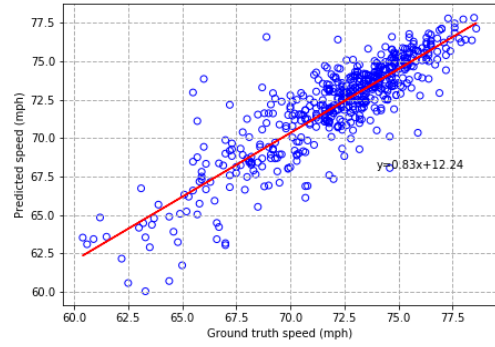
(a) METANET



(b) METANET-EKF



(c) GP



(d) PRGP-METANET

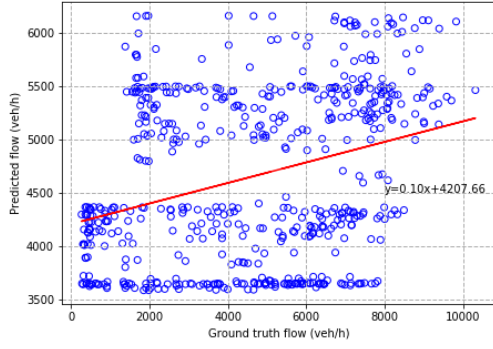
Figure 10: Comparison between speed estimation and the ground truth under missing data in Case I

5.2.2. Robustness Study

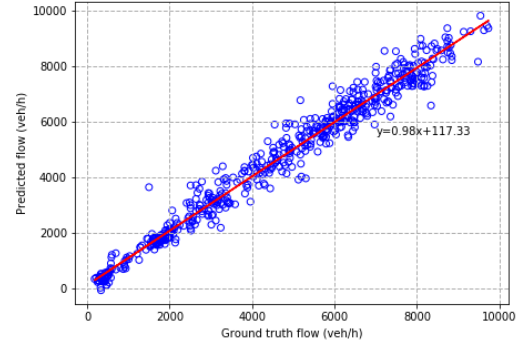
The METANET and METANET-EKF methods cannot handle the synthesized biased data. The comparison between them and imputation-capable methods, such as GP and PRGP, is not fair. Table 6 summarizes their estimation performance on the biased training data. The results show that the GP has limited resistance to high biased data, e.g., caused by traffic detector malfunctions. The PRGP model can greatly outperform pure GP by about $77.24 \text{ veh}/5\text{min}$ of RMSE and over 26.5% of MAPE in flow estimations. Hence, it can be concluded that the proposed PRML framework are much more robust than the pure ML models when the input data is subject to unobserved random noise. This is due to PRML's capability of adopting physical knowledge to regularized the ML training process. Fig. 11 compares the flow and speed estimation and the ground truth for the Case I.

Table 6: Comparison of the results of pure GP and the proposed PRGP under biased data in Case I

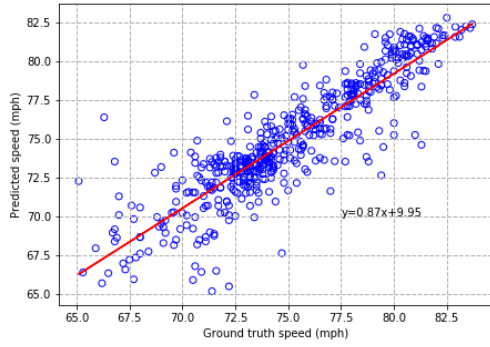
Method	RMSE of flow (veh/5min)	MAPE of flow	of	RMSE of speed (mph)	MAPE of speed	of
pure GP	127.24	86.50%		5.67	5.30%	
PRGP	45.66	14.60%		4.12	3.72%	



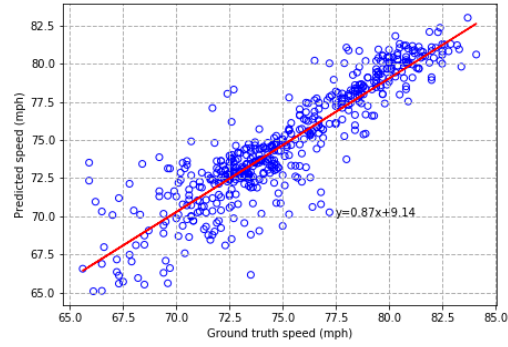
(a) GP flow



(b) PRGP flow



(c) GP speed



(d) PRGP speed

Figure 11: Comparison between flow estimations and the ground truth under biased and missing data in Case I

5.3. Numerical studies with Case II

5.3.1. Result Analysis

The comparable methods, METANET and METANET-EKF, are not designed to handle the data of the high missing rate. In each step, if the current detector data is missing, the measurement may use the last available observation and compromises the accuracy. Thus, the two methods are not tested in Case II. Table 7 shows the results of the proposed method and the conventional GP method in Case II. In comparison to the pure GP, the PRGP models can improve the accuracy of both flow and speed estimations, which is because PRGP can achieve a better estimation performance under the missing data condition. Fig. 12 compares the flow and speed estimation and the ground truth for the Case II.

Table 7: Comparison of the results of pure GP and the proposed PRGP under biased data in Case II

Method	RMSE of flow (veh/5min)	MAPE of flow	of	RMSE of speed (mph)	MAPE of speed	of
pure GP	42.22	12.57%		3.16	2.84%	
PRGP	36.25	10.81%		2.88	2.62%	

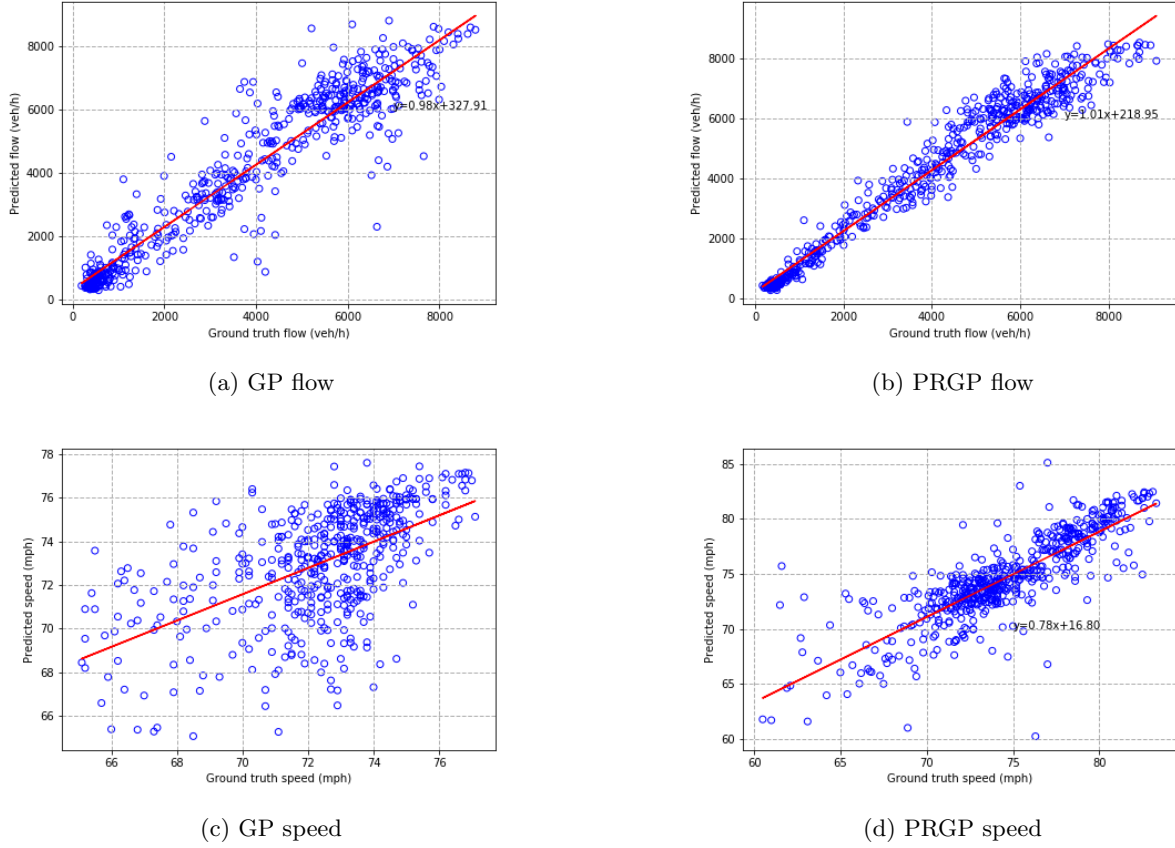


Figure 12: Comparison between flow estimations and the ground truth under missing data in Case II

5.3.2. Robustness Study

Table 8 summarizes their estimation performance on the noised training data. The results show that the GP has limited resistance to highly biased data. The PRGP model can greatly outperform pure GP by about $83.84 \text{ veh}/5\text{min}$ of RMSE and over 77.8% of MAPE in flow estimations. Fig. 13 compares the flow and speed of estimation and the ground truth. In comparison to the pure GP method, the proposed PRGP shows smaller variance in both the flow and speed predictions and smaller intercepts and greater coefficients of the trend lines in both the flow and speed predictions.

Table 8: Comparison of the results of pure GP and the proposed PRGP under biased data in Case II

Method	RMSE of flow (veh/5min)	MAPE of flow	RMSE of speed (mph)	MAPE of speed
pure GP	122.90	88.81%	2.93	2.49%
PRGP	39.06	11.01%	6.14	7.81%

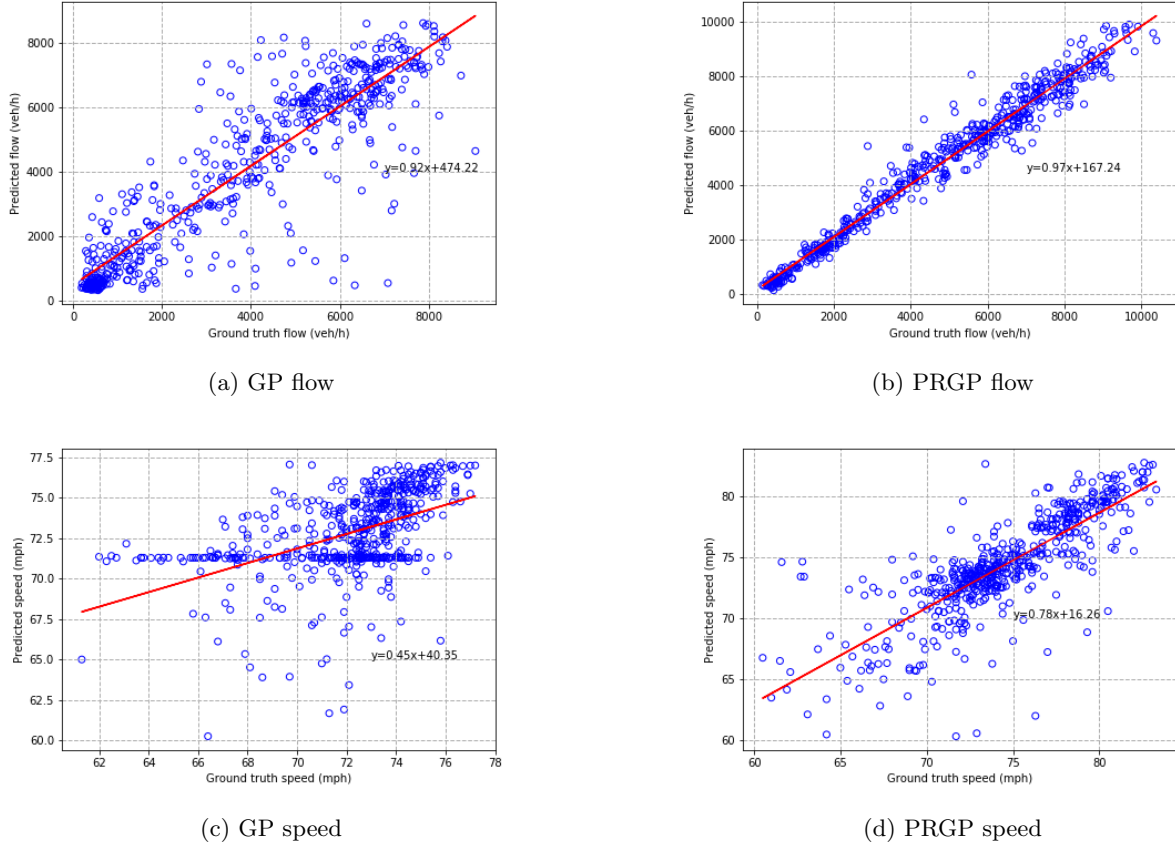


Figure 13: Comparison between flow estimations and the ground truth under biased and missing data in Case II

6. Conclusions and Future Research Directions

In the literature, traffic flow models have been well developed to explain the traffic phenomena, however, have theoretical difficulties in stochastic formulations and rigorous estimation. In view of the increasing availability of data, the data-driven methods are prevailing and fast-developing, however, have limitations of lacking sensitivity of irregular events and compromised effectiveness in sparse data.

To address the issues of both methods, an assimilation-imputation hybrid method to take the advantages of both methods is investigated. The data imputation is handled by the Gaussian Process (GP) considering the missing data and measure noise. To leverage the existing traffic flow models, a physics regularized Gaussian process (PRGP) is proposed to encode the physical knowledge in the Bayesian inference structure as the shadow Gaussian process. The physics models is encoded as the GP to regularize the conventional constraint-free Gaussian process as a soft constraint. To estimate the proposed PRGP, a posterior regularized inference algorithm is derived and implemented. A preliminary real-world case study is conducted on PeMS detection data collected from a freeway segment in Utah and the influential discrete traffic flow models and estimation methods are tested. In comparison to the pure machine learning methods and pure physical models, the numerical results justify the effectiveness and the robustness of the proposed method. In comparison to the pure physical models, the pure machine learning methods show better performance under the scenario of undetected locations. In the same testing scenarios, the proposed PRGP methods show similar performance as the pure GP. In comparison to the pure GP, the proposed PRGP show superior accuracy when the partial training data is biased due to unpredictable errors, such as detector malfunctions.

The future studies may explore more capabilities of this physics regularized machine learning, such as transfer learning for applying trained parameters in another location, incremental learning for training on multiple dataset with limited memory size, and ensemble learning for combining multiple models to strength the capability.

References

- Aw, A., Rascle, M., 2000. Resurrection of "second order" models of traffic flow. *SIAM journal on applied mathematics* 60, 916–938.
- Bekiaris-Liberis, N., Roncoli, C., Papageorgiou, M., 2016. Highway traffic state estimation with mixed connected and conventional vehicles. *IEEE Transactions on Intelligent Transportation Systems* 17, 3484–3497.
- Bishop, C.M., 2006. *Pattern recognition and machine learning*. springer.
- Chen, C., Kwon, J., Rice, J., Skabardonis, A., Varaiya, P., 2003a. Detecting errors and imputing missing data for single-loop surveillance systems. *Transportation Research Record* 1855, 160–167.
- Chen, Z., et al., 2003b. Bayesian filtering: From kalman filters to particle filters, and beyond. *Statistics* 182, 1–69.
- Daganzo, C.F., 1994. The cell transmission model: A dynamic representation of highway traffic consistent with the hydrodynamic theory. *Transportation Research Part B: Methodological* 28, 269 – 287.
- Daganzo, C.F., 1995. Requiem for second-order fluid approximations of traffic flow. *Transportation Research Part B: Methodological* 29, 277–286.
- Del Castillo, J., Pintado, P., Benitez, F., 1994. The reaction time of drivers and the stability of traffic flow. *Transportation Research Part B: Methodological* 28, 35–60.
- Duan, Y., Lv, Y., Liu, Y.L., Wang, F.Y., 2016. An efficient realization of deep learning for traffic data imputation. *Transportation research part C: emerging technologies* 72, 168–181.
- Fountoulakis, M., Bekiaris-Liberis, N., Roncoli, C., Papamichail, I., Papageorgiou, M., 2017. Highway traffic state estimation with mixed connected and conventional vehicles: Microscopic simulation-based testing. *Transportation Research Part C: Emerging Technologies* 78, 13–33.
- Ganchev, K., Das, D., 2013. Cross-lingual discriminative learning of sequence models with posterior regularization, in: *Proceedings of the 2013 Conference on Empirical Methods in Natural Language Processing*, pp. 1996–2006.
- Ganchev, K., Gillenwater, J., Taskar, B., et al., 2010. Posterior regularization for structured latent variable models. *Journal of Machine Learning Research* 11, 2001–2049.
- Gazis, D., Liu, C., 2003. Kalman filtering estimation of traffic counts for two network links in tandem. *Transportation Research Part B: Methodological* 37, 737–745.
- Gazis, D.C., Knapp, C.H., 1971. On-line estimation of traffic densities from time-series of flow and speed data. *Transportation Science* 5, 283–301.

- Göttlich, S., Ziegler, U., Herty, M., 2013. Numerical discretization of hamilton–jacobi equations on networks. *Networks & Heterogeneous Media* 8, 685.
- He, L., Gillenwater, J., Taskar, B., 2013. Graph-based posterior regularization for semi-supervised structured prediction, in: *Proceedings of the Seventeenth Conference on Computational Natural Language Learning*, pp. 38–46.
- Hoogendoorn, S.P., Bovy, P.H., 2001. State-of-the-art of vehicular traffic flow modelling. *Proceedings of the Institution of Mechanical Engineers, Part I: Journal of Systems and Control Engineering* 215, 283–303.
- Jabari, S.E., Liu, H.X., 2012. A stochastic model of traffic flow: Theoretical foundations. *Transportation Research Part B: Methodological* 46, 156–174.
- Kingma, D.P., Ba, J., 2014. Adam: A method for stochastic optimization. *arXiv preprint arXiv:1412.6980*.
- Lebacque, J.P., 1996. The godunov scheme and what it means for first order traffic flow models, in: *Transportation and traffic theory. Proceedings of the 13th international symposium on transportation and traffic theory, Lyon, France, 24-26 JULY 1996*.
- Lebacque, J.P., Mammar, S., Salem, H.H., 2007. Generic second order traffic flow modelling, in: *Transportation and Traffic Theory 2007. Papers Selected for Presentation at ISTTT17 Engineering and Physical Sciences Research Council (Great Britain) Rees Jeffreys Road Fund Transport Research Foundation TMS Consultancy Ove Arup and Partners, Hong Kong Transportation Planning (International) PTV AG*.
- Li, L., Li, Y., Li, Z., 2013. Efficient missing data imputing for traffic flow by considering temporal and spatial dependence. *Transportation research part C: emerging technologies* 34, 108–120.
- Libbrecht, M.W., Hoffman, M.M., Bilmes, J.A., Noble, W.S., 2015. Entropic graph-based posterior regularization: Extended version, in: *Proceedings of the International Conference on Machine Learning*.
- Lighthill, M.J., Whitham, G.B., 1955. On kinematic waves ii. a theory of traffic flow on long crowded roads. *Proceedings of the Royal Society of London. Series A. Mathematical and Physical Sciences* 229, 317–345.
- Lu, Y., Yang, X., Chang, G.L., 2014. Algorithm for detector-error screening on basis of temporal and spatial information. *Transportation Research Record* 2443, 40–48.
- Michalopoulos, P.G., Yi, P., Lyrintzis, A.S., 1993. Continuum modelling of traffic dynamics for congested freeways. *Transportation Research Part B: Methodological* 27, 315–332.
- Mihaylova, L., Boel, R., 2004. A particle filter for freeway traffic estimation, in: *2004 43rd IEEE Conference on Decision and Control (CDC)(IEEE Cat. No. 04CH37601)*, IEEE. pp. 2106–2111.
- Mihaylova, L., Boel, R., Hegiy, A., 2006. An unscented kalman filter for freeway traffic estimation, *IFAC*.
- Ni, D., Leonard, J.D., 2005. Markov chain monte carlo multiple imputation using bayesian networks for incomplete intelligent transportation systems data. *Transportation research record* 1935, 57–67.
- Papageorgiou, M., 1998. Some remarks on macroscopic traffic flow modelling. *Transportation Research Part A: Policy and Practice* 32, 323–329.

- Papageorgiou, M., Blosseville, J.M., Hadj-Salem, H., 1989. Macroscopic modelling of traffic flow on the boulevard périphérique in paris. *Transportation Research Part B: Methodological* 23, 29–47.
- Payne, H., 1971. Models of freeway traffic and control. *mathematical models of public systems*.
- Polson, N., Sokolov, V., 2017a. Bayesian particle tracking of traffic flows. *IEEE Transactions on Intelligent Transportation Systems* 19, 345–356.
- Polson, N.G., Sokolov, V.O., 2017b. Deep learning for short-term traffic flow prediction. *Transportation Research Part C: Emerging Technologies* 79, 1–17.
- Rasmussen, C.E., 2003. Gaussian processes in machine learning, in: *Summer School on Machine Learning*, Springer. pp. 63–71.
- Richards, P.I., 1956. Shock waves on the highway. *Operations research* 4, 42–51.
- Seo, T., Bayen, A.M., Kusakabe, T., Asakura, Y., 2017. Traffic state estimation on highway: A comprehensive survey. *Annual reviews in control* 43, 128–151.
- Smith, B.L., Scherer, W.T., Conklin, J.H., 2003. Exploring imputation techniques for missing data in transportation management systems. *Transportation Research Record* 1836, 132–142.
- Song, Y., Zhu, J., Ren, Y., 2016. Kernel bayesian inference with posterior regularization, in: *Advances in Neural Information Processing Systems*, pp. 4763–4771.
- Szeto, M.W., Gazis, D.C., 1972. Application of kalman filtering to the surveillance and control of traffic systems. *Transportation Science* 6, 419–439.
- Tak, S., Woo, S., Yeo, H., 2016. Data-driven imputation method for traffic data in sectional units of road links. *IEEE Transactions on Intelligent Transportation Systems* 17, 1762–1771.
- Tan, H., Feng, G., Feng, J., Wang, W., Zhang, Y.J., Li, F., 2013. A tensor-based method for missing traffic data completion. *Transportation Research Part C: Emerging Technologies* 28, 15–27.
- Tan, H., Wu, Y., Cheng, B., Wang, W., Ran, B., 2014. Robust missing traffic flow imputation considering nonnegativity and road capacity. *Mathematical Problems in Engineering* 2014.
- Tang, J., Zhang, G., Wang, Y., Wang, H., Liu, F., 2015. A hybrid approach to integrate fuzzy c-means based imputation method with genetic algorithm for missing traffic volume data estimation. *Transportation Research Part C: Emerging Technologies* 51, 29–40.
- Wang, Y., Papageorgiou, M., 2005. Real-time freeway traffic state estimation based on extended kalman filter: a general approach. *Transportation Research Part B: Methodological* 39, 141–167.
- Wang, Y., Papageorgiou, M., Messmer, A., 2007. Real-time freeway traffic state estimation based on extended kalman filter: A case study. *Transportation Science* 41, 167–181.
- Wang, Z., Xing, W., Kirby, R., Zhe, S., 2020. Physics regularized gaussian processes. *arXiv preprint arXiv:2006.04976* .
- Whitham, G., 1975. *Linear and nonlinear waves*. Modern Book Incorporated.

- Wong, G., Wong, S., 2002. A multi-class traffic flow model—an extension of lwr model with heterogeneous drivers. *Transportation Research Part A: Policy and Practice* 36, 827–841.
- Work, D.B., Tossavainen, O.P., Blandin, S., Bayen, A.M., Iwuchukwu, T., Tracton, K., 2008. An ensemble kalman filtering approach to highway traffic estimation using gps enabled mobile devices, in: 2008 47th IEEE Conference on Decision and Control, IEEE. pp. 5062–5068.
- Wu, Y., Tan, H., Qin, L., Ran, B., Jiang, Z., 2018. A hybrid deep learning based traffic flow prediction method and its understanding. *Transportation Research Part C: Emerging Technologies* 90, 166–180.
- Yin, W., Murray-Tuite, P., Rakha, H., 2012. Imputing erroneous data of single-station loop detectors for nonincident conditions: Comparison between temporal and spatial methods. *Journal of Intelligent Transportation Systems* 16, 159–176.
- Yuan, Y., Yang, X.T., Zhang, Z., Zhe, S., 2020. Macroscopic traffic flow modeling with physics regularized gaussian process: A new insight into machine learning applications. arXiv preprint arXiv:2002.02374 .
- Zhang, H.M., 2002. A non-equilibrium traffic model devoid of gas-like behavior. *Transportation Research Part B: Methodological* 36, 275–290.
- Zhong, M., Lingras, P., Sharma, S., 2004. Estimation of missing traffic counts using factor, genetic, neural, and regression techniques. *Transportation Research Part C: Emerging Technologies* 12, 139–166.
- Zhu, J., Chen, N., Xing, E.P., 2014. Bayesian inference with posterior regularization and applications to infinite latent svms. *The Journal of Machine Learning Research* 15, 1799–1847.